Proceedings of the ASME 2009 International Design Engineering Technical Conferences &
Computers and Information in Engineering Conference
IDETC/CIE 2009
August 30 - September 2, 2009, San Diego, California, USA

DETC2009-86247

AN INERTIALLY-ACTUATED PASSIVE DYNAMIC STEP CLIMBING WHEELED ROBOT

John Humphreys (Contact Author)
RoMeLa: Robotics & Mechanisms Lab
Mechanical Engineering Department
Virginia Polytechnic Institute and State University
Blacksburg, VA 24061
E-mail: jch@vt.edu

Dr. Dennis Hong
RoMeLa: Robotics & Mechanisms Lab
Mechanical Engineering Department
Virginia Polytechnic Institute and State University
Blacksburg, VA 24061
E-mail: dhong@vt.edu

ABSTRACT

For their inherent stability and simplicity, wheeled robots are very common in robotics applications – but a major drawback of wheeled robots is their inability to navigate over large obstacles or steps without assistance. Active systems that have been designed for use on wheeled robots to lift the robot over a step – such as USU's T3 and Virginia Tech's IMPASS – are effective, but are limited due to the size, cost, and power required for the additional actuators. A novel, inertially actuated, passive dynamic system, excited by the motion of the robot, is introduced to allow a wheeled robot to "pop a wheelie" on each axle and hop over a step. The system investigated here is a sliding mass-spring that shifts forward and backward based on the acceleration of the base robot. By coordinating the acceleration and deceleration of the robot, the front wheels can lift over a step and the rear wheels can be pulled up afterward – both actions being a product of inertial actuation. Key advantages of this system are that the design is simple, cost-effective, and can be adjusted and retrofit to a different wheeled robot in the future with little effort. This paper presents the development of a novel inertially actuated, passive dynamic step climbing wheeled robot. Derivations of the dynamic model of the inertially actuated system are given and a computer simulation and experiments of an implementation of this sliding mass system are presented, followed by conclusions with possibilities for future work.

INTRODUCTION

Wheeled robots are common in robotics applications, likely due to their simplicity and inherent stability when at least three wheels are present. Unlike robots that rely on a coordinated effort of legs to move, robots on wheels require very little design effort in order to maintain stability. Many wheeled robots have the need to climb a step: wheeled airport security robots that patrol the facility [1] are limited to moving along flat and slightly inclined surfaces. However, if the security robot needs to climb a curb and a ramp is not nearby, a possible security risk could go undetected. For situations like this where a robot needs the ability to climb a step immediately, some type of design is required to allow this maneuver.

While other robotic platforms, such as legged robots and some snake-like robots, are able to surmount large steps by manipulating themselves to rise up, wheeled robots are limited to flat surfaces and small steps. A wheeled robot can naturally climb steps that are lower than the radius of the robot's tires [2], but larger steps are insurmountable by basic friction contact of the wheels on the step. Robotic platforms have been designed to allow wheeled robots to climb steps [3-12], but these platforms rely on additional actuators, such as motors or hydraulic systems. For these options, extra power and added processing for control and coordination of these actuators are needed for the extra degrees of freedom.

We present a novel approach to climbing large steps with a wheeled robot utilizing a passive dynamic, inertially actuated sliding mass. This technique involves attaching a passive system that is inertially actuated to allow the robot to climb a step without directly controlling the mass. Before discussing the dynamics involved in this system, a proper introduction to the concept of *passive dynamics* and what this term generally applies to is required. Passive dynamics were first realized [13] as a more efficient walking pattern that takes advantage of gravity and the natural swing of legs instead of spending effort to actively manipulate legs for walking. In contrast to this original idea of passive dynamics, this research presents an idea of inertially actuated passive dynamics – which means a system is actuated through accelerations of a separate entity and is not directly controlled.

A simple implementation of inertially actuated passive dynamics is a spring-mass slider, which will be the main platform under investigation. In short, a sliding mass on top of a robot is pushed backward, during the robot's acceleration, from inertial forces and compresses a spring that is fixed to the sliding mass and the robot. This shift in the center of gravity location and coupled spring force can help lift the front wheels of the robot off the ground, essentially forcing the robot into a "wheelie". Once the front wheels contact the top of the step, braking causes a change in momentum that will slide the mass forward and stretch the spring. If done appropriately, this action can pop up the rear wheels over the step and allow the robot to have successfully climbed a step. There are other possible implementations of an inertially actuated passive dynamic system – such as an inverted pendulum – but a sliding mass system was deemed to be more practical, more stable, and simpler to implement.

This paper will present a detailed analysis of these effects, showing how these coupled reactions will allow a robot to pass its wheels over a step without actively interacting with the step. Dynamic simulations that were created will be discussed with respect their ability to design a working prototype

DYNAMIC MODEL OF STEP CLIMBING

Inertially Actuated Step Climbing Process

A diagram of the proposed design is shown in Figure 1. By adding a mass-spring slider on top of the robot at a predetermined height, the required accelerations to climb a step can be significantly reduced for both *lift-off* ("wheelie" on rear axle) and *pop-up* ("wheelie" on front axle) phases of step climbing. The center of gravity (COG) that is shown is for the base robot and is fixed. The overall COG of the system will change as the sliding mass moves, but the COG shown in Figure 1 is not affected by this motion and is at a constant position.

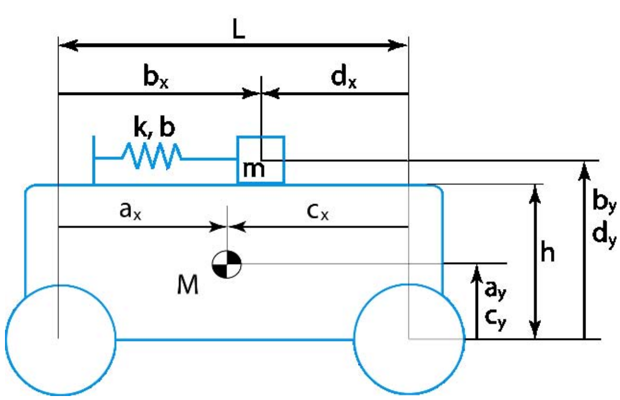

Figure 1: Diagram of a robot with a mass-spring slider attached to facilitate step-climbing.

While the mass addition changes the dynamics, an appropriate selection of mass, height, and spring stiffness will increase the robot's ability to rotate on both axles. Since the mass-slider will be added above the base robot, the effective center of mass will be raised. By using a spring to allow the mass to slide, the effective center of mass can shift forward and backward with the sliding mass. In addition to these effects, the deflection of the spring adds an extra torque on the robot to assist in the robot's rotation. A diagram of the step-climbing process for a wheeled robot with an inertially actuated sliding mass is shown in Figure 2.

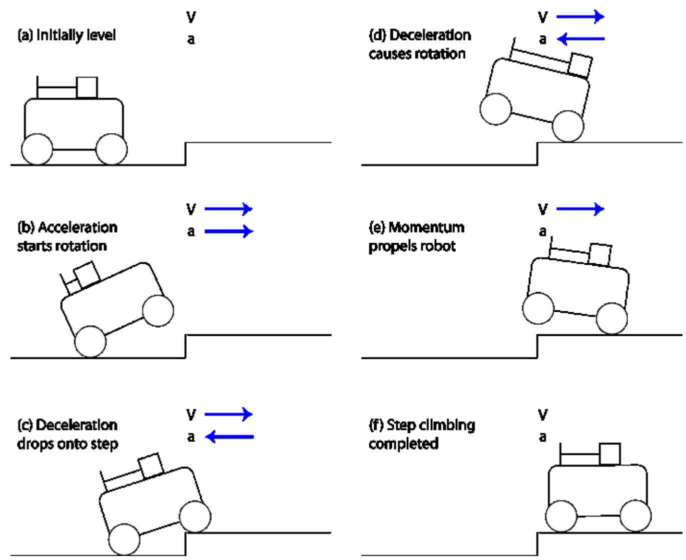

Figure 2: Diagram showing how an inertially actuated sliding mass can help a robot hop over a step.

For this inertially actuated step climbing process, the robot's acceleration causes the mass to slide back and compress the spring (see Fig 2b). This accomplishes two things – the center of gravity slides backward and an inertially induced reaction force is created in the spring that pushes back on the robot. When the robot is near the step (see Fig 2c), deceleration of the robot propels the mass forward and reverses the effects created during the lift-off. Now, the center of gravity is shifted forward and the inertial forces stretch the spring, which pulls forward on the robot. After the rear wheels are lifted as a result of this torque (see Fig 2d), the robot will use any forward momentum remaining and roll over the step before the rear wheels fall back down (see Fig 2e).

With the proper design and operational parameters, the spring-mass slider can both raise and shift the center of mass in order to aide in rotating the robot as well as create an additional reaction force from the spring compression. These changes allow for moderate accelerations to be used in both phases of the step-climbing process. The following sections will discuss the dynamics of the robotic system in each phase of step-climbing. These derivations will assume the properties of the base robot are fixed, so only parameters of the passive dynamic platform can be tuned to enable step climbing.

Sliding Mass Dynamics during Lift-off

A close-up view of the mass-slider and its associated reaction forces are shown in Figure 3. The mass is rotated at an angle of θ because of the robot's rotation, though the equation to compute this rotation has not been shown, yet. The initial condition for θ is 0^o, since the robot will be assumed to start on a flat surface. Lines are drawn to the rear axle, point O, about which the robot is rotating.

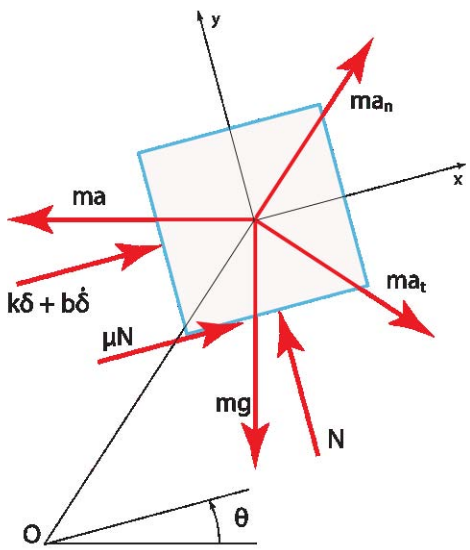

Figure 3: Free body diagram of the mass-slider during the lift-off phase

The reaction forces from the spring are dependent on the spring deflection, δ, which is positive in compression. The spring force causes a torque about the rear axle, helping the robot to lift its front wheels if the spring is compressed (δ > 0). Also, a positive deflection reduces the negative effect of the slider's mass on the total torque at the rear axle, which will be discussed in the next subsection. From these two effects, a larger, positive spring deflection is advantageous to helping the robot rotate on its rear axle. A summation of forces in the local-horizontal direction yields the equation of motion of the mass-slider, shown in Equation 1,

$$\begin{aligned} m\ddot{\delta} &= mg\sin\theta + ma\cos\theta - k\delta - b\dot{\delta} \\ &\quad - \mu\left(sign\dot{\delta}\right)\left(mg\cos\theta - ma\sin\theta\right) \\ &\quad - m\alpha\left(b_y + b_x\mu\left(sign\,\dot{\delta}\right)\right) \\ &\quad + m\omega^2\left(b_y\mu\left(sign\,\dot{\delta}\right) - b_x\right) \end{aligned} \tag{1}$$

where variables can be defined using Figure 1 or Figure 3. Minor details such as spring damping, b, and friction between the sliding mass and the base robot, μ, are shown for completeness. The assumption is being made that the friction between the sliding mass and the robot is low enough that the slider does indeed move and is not held by friction. From the equation of motion for the mass-slider and knowing that a larger deflection value, δ, is helpful for the lift-off process, several design parameters can be adjusted. The first four components of Equation 1 are largely the most significant, while the last three are smaller details that will be ignored for this design discussion – this simplification is justified through simulations [14]. These effects are important and are included in the full dynamic model but are not significant when tuning design values. Using these assumptions, Equation 2,

$$\ddot{\delta} \approx g\sin\theta + a\cos\theta - \frac{k}{m}\delta - \frac{b}{m}\dot{\delta} \tag{2}$$

shows a simplified form of Equation 1 that is useful for designing the spring-mass system. This simplification should not be used as an approximation of the system dynamics; the only functional use of this equation is to investigate how changing certain design values *generally* changes the deflection of the mass-spring system.

Equation 2 shows that increasing the slider mass will tend to increase deflection of the spring so long as the extra mass does not reduce the acceleration available. Also, a lower spring constant and damping value will lead to larger spring deflections. These spring properties are completely independent of other parameters and can be varied without concern for worsening the effects from other values. Important to note is that for typical robot rotations and accelerations, larger rotation values lead to larger spring deflections – indicating the limiting stage is the initial rotation of the robot.

Rotating Robot Dynamics during Lift-off

With the dynamics of the mass-slider defined, the rotation of the robot during the lift-off phase can be analyzed. Removing the mass-slider, a free-body diagram of the robot is shown in Figure 4.

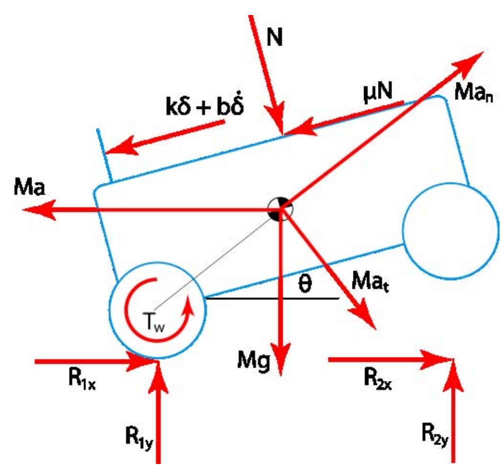

Figure 4: Free body diagram of the robot during the lift-off phase

The mass-slider has been replaced by the reaction forces that were created by its addition: a normal force from the mass contacting the robot base, a spring force where the spring connects to the robot base, and a friction force that is dependent on the mass velocity direction.

Evaluation of the torque about the rear axle will show the robot's ability to lift its front wheel during acceleration. Note that the reaction forces R_{2x} and R_{2y} only exist when the front wheel contacts the ground, but are shown for completeness. To find the rotational dynamics of the robot about its rear axle, the torques created from the reaction forces must be analyzed. A summation of these torques, shown in Equation 3, indicate how capable the robot is of rotating,

$$\begin{aligned} I_1\alpha_1 &= (k\delta + b\dot{\delta})b_y + Ma(a_x \sin\theta + a_y \cos\theta) \\ &- Mg(a_x \cos\theta - a_y \sin\theta) - M\alpha L_M^2 \\ &+ (mg\cos\theta + m\alpha b_x - m\omega^2 b_y - ma\sin\theta)(\mu h(sign\,\dot{\delta}) - b_x) \\ &+ R_{2y}L + T_w \end{aligned} \quad (3)$$

where variables can be defined using Figure 1 or Figure 4. The mass, M, and center of mass location of the robot's base, a_x and a_y, are essentially fixed, though they may vary depending on the rigid structure needed to add the mass-slider. The sliding mass moves and changes the effective center of gravity location for the entire robot, but the sliding mass location is denoted using b_x and b_y and this position doesn't affect the center of gravity of the base robot. The vertical reaction forces at the tires are not constant values. Rather, these reactions vary by assuming the tires to be spring-damper systems. The reaction at the front axle is coupled into the rotation equation – deflection of the tire occurs during negative rotation. The deflection at the rear axle is modeled as a separate system and will be discussed later.

The rotational dynamics expressed in Equation 3 can be simplified [14] for design parameter selection. Equation 4 shows this reduced equation,

$$I_1\alpha_1 = (k\delta + b\dot{\delta})b_y + (-mg\cos\theta + ma\sin\theta)b_x + T' \quad (4)$$

where terms that are relatively small or consist of parameters of the base robot that are fixed are lumped into a temporary variable, *T'*. The configurable parameters of the design remain the spring stiffness (k), mass of the slider (m), and position of the slider (b_x and b_y).

Equation 4 indicates that to rotate the robot on its rear axle, the spring stiffness and slider height values should be increased while the horizontal position of the slider should be reduced (move the slider back) and slider should be lighter. The adjustments to the spring stiffness and slider mass are in contrast to the knowledge of the sliding mass dynamics, so a balance between the two is necessary. However, adjusting these design parameters as specified by the sliding mass dynamics (lower spring stiffness and higher sliding mass) generally outweigh the effects shown for the rotating robot. Inspection of terms that involve the robot's rotation, θ, show that the rotation of the robot is advantageous to helping the robot to continue to rotate. This positive feedback relationship shows the limiting point for the robot's rotation is when the robot is still flat.

Sliding Mass Dynamics during Pop-up

The dynamics of the pop-up action are very similar to those for the lift-off action, though the center of rotation is now at the front axle. A free body diagram of the sliding mass during pop-up is shown in Figure 5. Lines indicate the relationship between the sliding mass and the front axle at point Q. A force balance on the slider in the local-horizontal direction is shown in Equation 5,

$$\begin{aligned} m\ddot{\delta} &= mg\sin\theta + ma\cos\theta - k\delta - b\dot{\delta} \\ &- \mu(sign\dot{\delta})(mg\cos\theta - ma\sin\theta) \\ &- m\alpha(d_y - d_x\mu(sign\,\dot{\delta})) \\ &+ m\omega^2(d_y\mu(sign\,\dot{\delta}) + d_x) \end{aligned} \quad (5)$$

where variables are defined from Figure 1 or Figure 5. The main differences evident in the sliding mass equation during pop-up are that distances are now denoted using d_x and d_y variables, which are referenced to the front axle, and two sign changes in the rotational accelerations to account for reversed rotation.

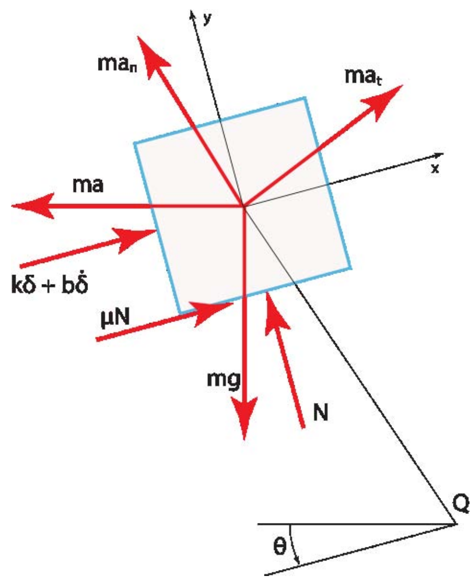

Figure 5: Free body diagram of the sliding mass during the pop-up phase

Making simplifications to the dynamics based on significance with respect to other values [14], Equation 6 was created,

$$\ddot{\delta} \approx g\sin\theta + a\cos\theta - \frac{k}{m}\delta - \frac{b}{m}\dot{\delta} \quad (6)$$

which shows how spring deflection depends on the most important terms from Equation 5. This reduced relationship is exactly the same as was derived for the sliding mass during lift-off. Since the equations are equivalent, the lessons available for the sliding mass during pop-up are similar to those from the lift-off process. A lower spring stiffness and larger sliding mass are advantageous to the sliding mass stretching the spring – assuming the sliding mass is able to begin sliding forward. When the spring is in compression ($\delta > 0$), these options are reversed; but the negative effects during this phase are outweighed by the benefits during spring tension ($\delta < 0$). As before, inspection of the effects of the robot's rotation, θ in Equation 6 show the limiting point for the sliding mass moving forward is when the rear wheel is still on the ground

Rotating Robot Dynamics during Pop-up

Having defined the dynamics of the sliding mass, the actual rotation of the robot during the pop-up phase can be established. Using a free body diagram of the robot when rotating about its front axle, shown in Figure 6, the effects of each reaction force on the pop-up action were derived for Equation 7,

$$
\begin{aligned}
I_2\alpha_2 &= \left(k\delta + b\dot{\delta}\right)d_y - Ma\left(c_x \sin\theta - c_y \cos\theta\right) \\
&+ Mg\left(c_x \cos\theta + c_y \sin\theta\right) - M\alpha L_{M'}^2 \\
&+ \left(mg\cos\theta - m\alpha d_x - m\omega^2 d_y - ma\sin\theta\right)\left(\mu h\left(sign\,\dot{\delta}\right) + d_x\right) \\
&- R_{1y}L + T_w \qquad (7)
\end{aligned}
$$

where variables are defined via Figure 1 or Figure 6. With the tires modeled as spring-dampers, the vertical reaction force at the rear axle, R_{1y}, varies based on the actual deflection of the tire.

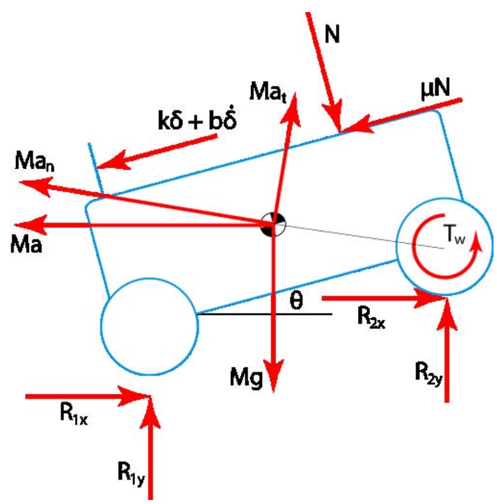

Figure 6: Free body diagram of the robot during the pop-up phase

The main differences from the lift-off equation are sign changes to account for rotation about an elevated point (the front wheel on top of the step) and the use of variables *c* and *d* to reference distances to the front axle. The horizontal reaction force at the rear tires disappears once the rear wheels begin to pop up, so it doesn't warrant inclusion in the dynamics of the robot's rotation.

By grouping terms from Equation 7 that are either fixed values or very small compared to other terms (as explained externally [14]) into a temporary value, T', Equation 8 was created,

$$I_2\alpha_2 = \left(k\delta + b\dot{\delta}\right)d_y + \left(mg\cos\theta - ma\sin\theta\right)d_x + T' \qquad (8)$$

in order to better understand the relationship between the design values and the robot's rotation. During pop-up, a negative angular acceleration is desired to pop the rear wheels up towards a horizontal, no-rotation condition. To achieve this, the spring stiffness (k), slider height (b_y), and slider mass (m) are again the terms able to be modified.

Like analysis of the lift-off phase, the effects of changing the spring stiffness and slider mass using Equation 8 are outweighed by the changes evident in the sliding mass dynamics. Therefore, increasing rotation of the robot is likely accomplished by reducing the spring constant and raising the slider mass – based on Equation 6 – and also by placing the sliding mass higher and further forward based on Equation 8. All of these adjustments assume that the robot is able to overcome the negative effects of a compressed spring to reap the benefits of a spring in tension. A final inspection of the robot's rotation, θ, in Equation 8, shows that the limiting point during the robot's rotation is when the rear wheels first raise off the ground.

Tire Deflection Model on Rotation Axle

The equations for the rotation of a robot during each phase of inertially actuated step climbing have been defined, including the tire deflection of half of the tires. By modeling the tires as spring-damper systems, the actual deflection of the tires can be simulated. This correction, however, only accounts for the tires that are not on the axle of rotation. The deflection of these tires is implemented in an independent set of equations. This section will present the deflection of the rear tire during lift-off. Modeling of the front wheel deflection during pop-up is very similar, so it is not shown.

The equilibrium force of the tire is first computed from a vertical force balance of the system in Figure 4, shown in Equation 9,

$$
\begin{aligned}
R_{1y,eq} &= \left(k\delta + b\dot{\delta}\right)\sin\theta + m\alpha\left(a_x \cos\theta - a_y \sin\theta\right) \qquad (9) \\
&- m\omega^2\left(a_x \sin\theta + a_y \cos\theta\right) + Mg - R_{2y} \\
&+ \left(mg\cos\theta + m\alpha b_x - m\omega^2 b_y - ma\sin\theta\right) \\
&* \left(\cos\theta + \mu\left(sign\dot{\delta}\right)\sin\theta\right)
\end{aligned}
$$

where variables have been defined in previous figures. This force represents the force that would be in the tire if the tire was in equilibrium and its deflection was not changing. Relating this equilibrium force to the actual force absorbed in the tire based on the current deflection results in an unbalanced force in the tire deflection. This unbalance force is then used in Equation 10 to find the "deflection acceleration" of the tire, $\ddot{\delta}_T$,

$$(m+M)\ddot{\delta}_T = F_{unbalance} \tag{10}$$

where the total mass of the robot is used to compute how quickly the tire deflects. Integration of this acceleration yields a new tire deflection for the next time step. This is a fairly simplified model of tire deflection with some imperfect assumptions, but the small correction to the robot's dynamic model helps to capture all aspects of an actual robot.

COMPUTER SIMULATION

To determine how the passive system can allow for step climbing by wheeled robots, a simulation was designed to model the system dynamics. Rather than using a software package, such as Matlab, that is already capable of simulating dynamic systems, a new simulation using C++ was created. By writing a custom simulation code, extra flexibility was allowed for modifying the simulation parameters and ensuring a firm understanding of the simulation process.

Implementing the equations derived previously and allowing for quick manipulation of data, an easy and effective simulation was created. The simulation uses a C++ graphics extension, OpenGL, to visualize the robot as it moves. This display shows a simplified model of the rotating robot, an indicator of the sliding mass position, and the location of the step.

Figure 7 shows an example of the window that is created during execution of the simulation. The screen simulates a camera fixed to the local position of the robot and moves with the robot. The robot stays centered in the window and rotates as necessary as the "world" moves across the view.

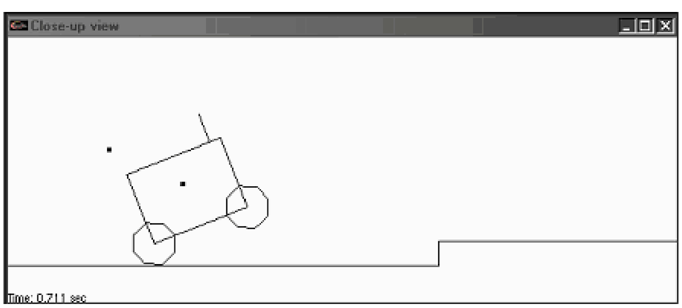

Figure 7: Example of the simulation display output.

In the graphics window, the base of the robot is displayed as two wheels and a rectangular body. The COG of the robot is shown as a black point inside the robot. Since this simulation is intended for a general wheeled robot, no further detail is necessary. A line extends from the base of the robot upwards to indicate the equilibrium height and horizontal position of the sliding mass. The black point above the robot in the image shows the actual position of the sliding mass at the current time as the mass oscillates around the equilibrium point.

By having this window visible, substantial detail of the entire process is available, including the rotation of the robot and position of the sliding mass. For a print-out of the system parameters during simulation, the simulation can write any data to file for later use. The inputs to the simulation include all variables in the dynamic models and an acceleration profile. The true input to a robotic system would be an electrical current or power draw, but this adjustment simplified the system and allowed the internal operation of the robot to be ignored. If a certain acceleration is attainable, the required power is inconsequential for this project.

The use of this simulation to design the robotic system is described as appropriate in the next section.

EXPERIMENTAL RESULTS

To expedite testing, a remote-control car was used as the base robotic platform for experiments. A 27 MHz radio controller that was provided with the car was used to control the robot instead of making significant modifications to enable tethered control or the use of an on-board controller. Using an accelerometer attached to the robot, the actual driving pattern of the robot can be tracked for comparison to simulations. By controlling the robot by hand and recording its acceleration, the internal dynamics of the robot (such as the required power draw and losses in the system) can be ignored and the dynamic simulation can be easily used.

To find the acceleration and deceleration limits of this robot, several acceleration tests of the system were performed. By applying full power during acceleration and deceleration and recording data from an accelerometer, a reasonable power limit can be estimated. With a small addition of mass (0.5 lbs) to simulate the added structure to support the sliding mass and a larger addition of weight (2.5 lbs) to simulate the sliding mass, a range of accelerations that can be expected while the sliding mass stretches the spring is apparent. All tests yielded the same conclusion – the acceleration of the robot during the step-climbing process will likely be between 3 m/s^2 and 5 m/s^2 and the deceleration of the robot will average between 3 m/s^2 and 6 m/s^2.

The first attempt at designing a step-climbing robot involved designing a robot using simulations, building the robot, and verifying that the simulations could match the actual rotation profile of the robot. Knowing that a very high sliding mass meant the robot would have an easier time rotating around its axles, in general, the first robot design was very tall. Once an acceleration profile was created in a simulation that showed this robot could climb the step, the actual sliding mass platform that would be installed on the base robot could be built.

The end result of this design is shown in Figure 8 – a wood block was formed to mount the top of the RC car and an aluminum platform was created to fit on top. A linear bearing was attached to the top of the platform and several blocks of aluminum were combined to form the mass of the slider. A spring is connected from the slider to a fixed bracket and is supported with a wood dowel that passes through the bracket. The platform was designed to be very simple but adjustable for easy design changes. The height of the platform, position of the spring bracket, and mass of slider are quickly adjustable. To cut weight, patterns were milled in the aluminum beams to minimize weight while ensuring structural stability. Since this design was being used to simply validate the simulations, the great height of the system was not a concern.

Figure 8: A robot equipped with a passive dynamic system to enable step-climbing to verify the design simulations

The design parameters of the actual robot that was created are shown in Table 1. These values are physical characteristics of the robot shown in Figure 8 and were measured directly from the system. The dimensions used were generated through iterating with the simulator until the step-climbing process was found successful. Since they were essentially generated through trial and error, these values are not optimized and merely present a system that should be capable of climbing a step.

Table 1: Design parameters for the robot used to validate simulations

M	2.01 kg
a_x	8.25 cm
a_y	19.1 cm
L	17.1 cm
h	48.3 cm
m	0.77 kg
b_{xo}	17.8 cm
b_y	53.3 cm
k	26 N/m

Since the actual robot was being controlled through a radio controller by hand, numerous tests were required to achieve step-climbing, though the process did eventually work. The robot was able to lift its front wheels over the step and decelerate enough to pop the rear wheels above the step. Since acceleration is limited at higher velocities, the robot could not begin at a large enough initial velocity for the momentum to carry the robot over the step while in the air. This limitation would likely not exist in a real robot that uses motors stronger than the default options for this RC car. Selections from a video that was taken of one successful test are shown in Figure 9. The process here follows the expectations outlined in Figure 2. A hand was kept near the robot at all times because of the difficulty controlling the system, but the actual contact was kept to a minimum. Frame (e) shows that the robot pulls its rear wheels high enough to get over the step, but Frame (f) indicates that the robot didn't continue forward quite enough to actually climb the step.

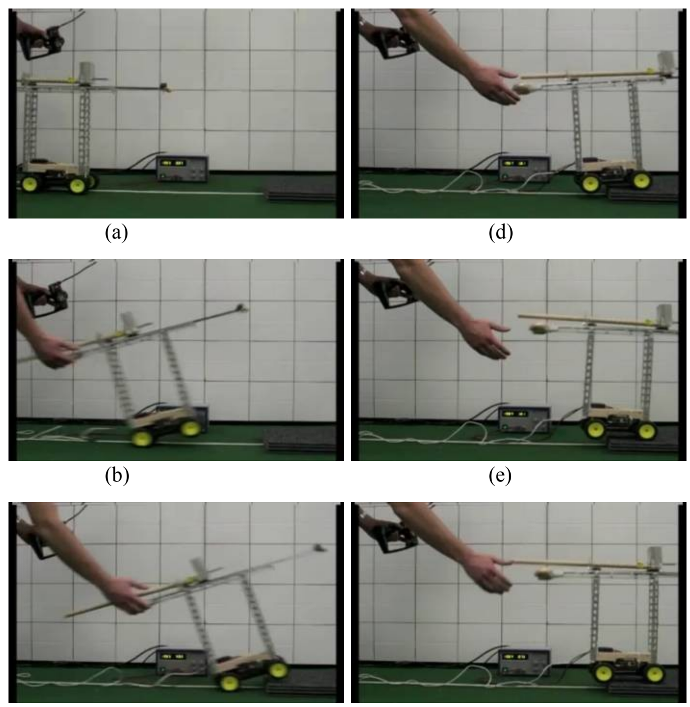

(a) (d)

(b) (e)

(c) (f)

Figure 9: Selections from video of the step-climbing process for an initial test of the inertially actuated system.

With the acceleration data and actual structure of the robot from this test, these parameters were then reused in the C++ simulation to see if the profile of the robot could be matched using a similar acceleration input. Figure 10 shows the acceleration profiles for the actual test and the simulation. The maroon plot is the actual acceleration data taken from experimentation. The orange plot is the highly-simplified acceleration model that was put into the C++ simulation. This acceleration profile was created by keeping the geometrical parameters of the robot constant and varying the acceleration in order to best match the rotation data taken from the test.

There are two reasons for not using the actual acceleration profile taken from the test and using this as the input to the dynamic simulation. First, looking at Figure 10 shows the acceleration data is very noisy and doesn't seem to agree with the input method. To control this robot, full power was given to accelerate the robot until the robot was near the step. Then, the

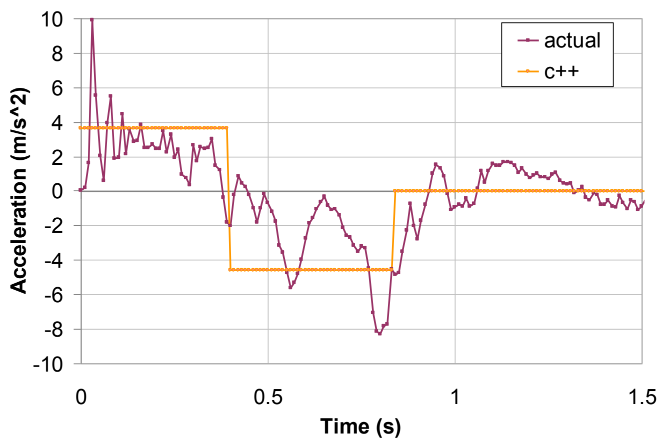

Figure 10: A plot of acceleration versus time for an actual test and a simulation.

robot was immediately put in reverse at full power. This input should show a relatively constant acceleration (which is evident) followed by a relatively constant deceleration (which is not the case). In addition, the large oscillations and spikes in the acceleration data raise questions about its accuracy.

Based on the acceleration tests that were performed on the base robot, the constant values of acceleration and deceleration used as the simplified input are within the ranges expected during the process. The actual acceleration profile, shown in Figure 10, also shows values within this range, though oscillations are significant in this data. These two factors mean that the magnitude of acceleration for the simplified model is reasonable. In addition, from Figure 10, the point where deceleration starts is nearly identical – around 0.4 seconds – for both the simulation acceleration and the experimental acceleration profiles.

The rotation profile of the robot from the actual test and from the simulation using the simplified acceleration input is shown in Figure 11. The actual rotation profile is again shown in the maroon plot and the C++ simulation data is the orange trend. The two plots match very well and share similar characteristics. A brief period of rotation lasts around 0.3 seconds, then the rotations speed up and the two profiles share similar maximum rotation values. Upon deceleration, the front wheels land on the step and the robot rotates backward to a nearly flat orientation, pauses, and then continues rotating far enough to raise the rear wheels over the step. The two cases diverge somewhat during this process, but the overall goal of climbing a step is accomplished in both situations.

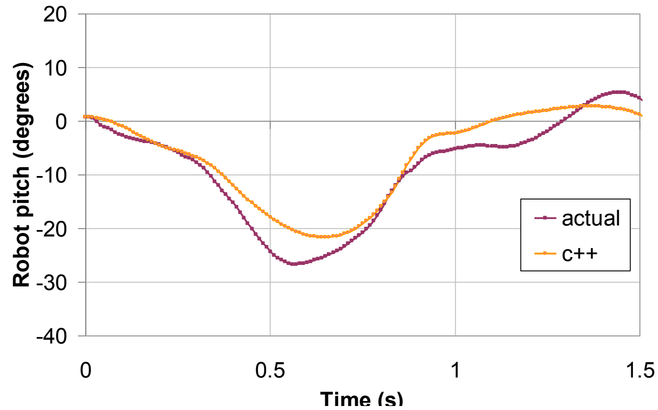

Figure 11: A plot of rotation versus time for the acceleration data in Figure 10.

After verifying the usefulness of the design simulations, further testing with the simulations resulted in a shorter, slightly optimized, step-climbing wheeled robot as defined in Table 2. From the original robot, only the slider height (b_y) and equilibrium position (b_x) needed to be adjusted. The other design parameters of the robot were held constant, while the acceleration profile of the system should be adjusted to account for the change in the overall dynamics.

Table 2: Design parameters of optimized robot

M	2.01 kg
a_x	8.3 cm
a_y	7.6 cm
L	17.1 cm
H	48.3 cm
M	0.77 kg
b_{xo}	15.2 cm
b_y	17.8 cm
K	26 N/m

Figure 12 shows the optimized wheeled robot experimentation and the sliding mass-spring system is attached on top. The wood block and aluminum platform were used only to raise and support the sliding mass. A wood dowel supports the spring from the inside to prevent buckling and the sliding mass is constrained to 1-D motion on a linear bear.

Figure 12: A wheeled robot used for testing with a sliding mass-spring system to enable step-climbing.

Testing for this robot was performed using a wireless manual controller, so excessive testing was required to effectively coordinate the acceleration and deceleration of the robot climb a step. To show that this sliding mass system increases the mobility of the robot, a step larger (1.625”) than the radius of the robot’s tires (1.5”) was used – since wheeled robots are able to roll over steps smaller than the tire radius. Figure 13 shows a selection of pictures during a successful trial. The series here matches the expectations from Figure 2, proving that the inertially actuated sliding mass is capable of facilitating step-climbing by a wheeled robot.

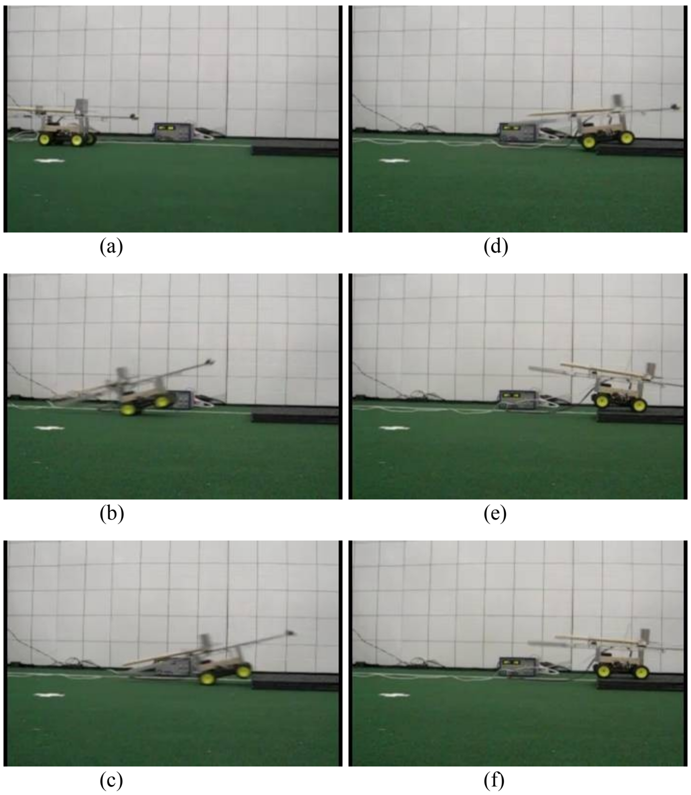

Figure 13: Selected images from video as a wheeled robot climbs a step.

Since this was a “proof of concept” experiment and was manually controlled, matching the rotation of profile of an actual test to a predicted test from the design simulations is difficult. Acceleration data was collected from the robot during tests and compared to results from a simulation using a simplified, linear acceleration model. The rotation profiles match well, following the same trends and reaching similar peak rotation values, though are not exact and indicate some discrepancy.

CONCLUSIONS

In this paper we have presented a novel, inertially-actuated, passive dynamic system that enables wheeled robots to climb steps that were previously impassable. A dynamic model of an inertially actuated sliding mass was derived and used to show how design parameters can be adjusted to allow a wheeled robot to hop over a step. A proper coordination of acceleration and deceleration of the robot must be attained, but this system can be tuned and retrofit to another wheeled robot to increase its mobility using the design guidelines that were discussed.

To verify that the dynamics have been fully understood, a simulation of the system was created. This simulation revealed the plausibility of the step-climbing process and also enabled the design of a sliding mass system to allow a wheeled robot to climb a step.

Experiments on a wheeled robot proved the sliding mass system to be effective. Video captured during testing agreed well with the predicted step-climbing process. Although comparisons between the experiments and simulations are limited (since the experiments were controlled manually), brief comparisons show the rotation profile of the robot to be similar between tests. In all, the experiments served as a “proof of concept” and confirmed that the sliding mass system that was designed could enable step-climbing via inertial actuation.

Since this was an initial investigation, future work on this project is plentiful. The dynamic model of the system could be improved to capture more details of the dynamics of the system – especially in the tire model. The simulations showed the system to be very sensitive to changes in the tire model, so improving those dynamics are integral to improving the overall system. Other areas of research that should be probed include designing an onboard feedback controller to guide the step-climbing process as well as investigating alternative inertially actuated systems, such as an inverted pendulum that is controlled through accelerations of the robot.

ACKNOWLEDGMENTS

We would like to recognize Derek Lahr and Karl Muecke for their contributions in conceiving the step-climbing process presented in this paper.

REFERENCES

[1] “KABOOM!! Setting off a bomb in the name of safety”, Feb 2008, National Research Council Canada <http://www.nrc-cnrc.gc.ca/eng/education/innovations/spotlight/kaboom.html>

[2] A. Wilhelm, W. Melek Sr., J. Huissoon, C. Clark, G. Hirzinger, N. Sporer, M. Fuchs, “Dynamics of Step-climbing with Deformable Wheels and Applications for Mobile Robotics”, Proceedings of the 2007 IEEE/RSJ International Conference on Intelligent Robots and Systems, November 2007, pp. 783-788.

[3] K.L. Moore, N.S. Flann, "A Six-Wheeled Omnidirectional Autonomous Mobile Robot," IEEE Control Systems Magazine, December 2000, pp. 53-66.

[4] D.R. Robinson, C. Wood, "Stair climbing capabilities of USU's T3 ODV mobile robot," Proceedings of SPIE, Vol. 4364 (2001).

[5] H. McGowen, “Navy omnidirectional vehicle (ODV) development and technology transfer opportunities,” Coastal Systems Station, Dahlgren Division, Naval Surface Warfare Division, unpublished report.

[6] M. Asama, M. Sato, H. Kaetsu, K. Ozaki, A. Matsumoto, and I. Endo, “Development of an omnidirectional mobile robot with 3 DOF decoupling drive mechanism,” Journal of the Robotics Society of Japan, vol. 14, no. 2, pp. 95-100, 1997 (in Japanese).

[7] S. Kimmel, D. Hong, “Software Architecture and Motion Planning for Traversing Obstructed Terrain with a Rimless Wheel with Individually Actuated Spokes”, KSEA US-Korean Conference on Science, Technology, and Entrepreneurship, Reston, VA, 2007

[8] D. Campbell, M. Buehler. “Stair Descent in the Simple Hexapod 'RHex',” Proceedings of the 2003 IEEE Int. Conf. on Robotics and Automation (ICRA).

[9] D.M. Helmick, S.I. Roumeliotis, M.C. McHenry, L. Matthies, "Multi-sensor, high speed autonomous stair climbing," Intelligent Robots and System, 2002. IEEE/RSJ International Conference on , vol.1, no., pp. 733-742 vol.1, 2002

[10] Y. Uchida, K. Furuichi, S. Hirose, “Consideration of stair-climbing performance of a six-wheeled off-road vehicle ‘HELIOS-V’”，Proc. 2nd Int. Symp. CLAWAR 99，383-391(1999)

[11] W.A. Lewinger, M.S. Watson, R.D. Quinn, "Obstacle Avoidance Behavior for a Biologically-Inspired Mobile Robot Using Binaural Ultrasonic Sensors," Proceeding of the IEEE/RSJ International Conference on Intelligent Robots and Systems (IROS'06), Beijing, China, October 9-13, 2006.

[12] “Futuristic Unmanned Ground Combat Vehicle Revealed”, Unmanned Systems Volume 24 No. 4, 2006

[13] T. McGeer, “Passive dynamic walking,” Int. J. Robot. Res., vol. 9, no. 2, pp. 62–82, 1990.

[14] J. Humphreys, “Development of an Inertially-Actuated Passive Dynamic Technique to Enable Single-Step Climbing by Wheeled Robots”, Masters Thesis, Virginia Polytechnic Institute and State University, 2008.